The Impact of Aspect Ratio, Characteristic Strength and Compression Rebars on the Shear Capacity of Shallow RC Beams

Ahmed A. Soliman [1, 2*] , Dina M. Mansour [1] , Ayman H. Khalil [2] , Ahmed Ebid [1]

[1] Department of Structural Engineering and Construction Management, Future University in Egypt, Egypt.

[2] Structural Engineering Department, Faculty of Engineering, Ain Shams University, Egypt.

Abstract

This paper investigates the impact of the aspect ratio, the characteristics strength of the concrete, and the compression steel ratio on the shear capacity of wide-shallow beams. An experimental program consists of seven specimens, including a control specimen, all tested under a three-point load test. Three specimens were considered for each parameter (the control specimen was included in all three variables). The experimental results were compared to the theoretical values of six different codes of practice; they were also analyzed to determine the ductility, stiffness, and dissipated energy of each specimen. The results indicated that the shear reinforcement was fully functioning until it yielded, with a minimum contribution of 55% of the total shear capacity of the specimens. The aspect ratio and the characteristic strength had a notable impact on the shear capacity of the specimens, while the compression steel ratio had a minor effect on the shear capacity, but it improved the stiffness and the ductility of the beams. Theoretical concrete shear strengths from design codes ranged between 77 and 163% of the experimental values; EN-1992 was the closest code to the experimental results. A comparison between the experimental results and predicted values using GP and EPR methods from previous research showed accuracies of 72% and 81%, respectively.

Keywords: Wide Beams; Shallow Beams; Shear Capacity; Experimental Study.

1. Introduction

Wide-shallow reinforced concrete beams are widely used in construction as they account for more architectural creativity through the increased clear height provided by them and their economic viability if they act as a concealed beam embedded in the slabs, which means easier and faster formwork. Shallow / wide beams were defined as beams whose widths are more than twice their depth (width / depth > 2) [1]. Stirrup usage in reinforced concrete wide beams and its effect on the shear capacity were not considered by the mainstream guidelines and codes of practice [2]. The American code of practice, ACI 314-2019, stated that if the beam depth is less than or equal to 10 inches (25.4 cm), it should be considered a shallow depth. At this depth, it is not required to satisfy the minimum shear reinforcement for the shallow wide beams [3], but in 2004, it was stated that for some types of wide beams, shear reinforcement is advised [4].

Different steel configurations in wide beams were investigated over the years. In 2020, several experimental investigations took place with notable conclusions. An experimental investigation that serves as a comparison between wide beams and conventional beams was conducted on fourteen specimens. As the depth of the wide beam increased, its behavior shifted to that of the conventional beam [5]. Two wide beam specimens were designed according to Eurocode 2 and the other according to the Saudi code of practice; 0.6 d was the most effective longitudinal spacing between the stirrups [6]. In 2021, an experimental investigation had four wide beam specimens tested with the

longitudinal spacing between stirrups as the only variable. It was concluded that as these spacings decreased, the shear capacity improved [7]. Another experimental investigation with seven wide beam specimens also focused on the longitudinal spacing between stirrups, but under eccentric loading, it was concluded that decreasing the spacing had a positive effect on crack control [8]. In 2022, two experimental investigations regarding the wide beams took two different approaches. Nine specimens with spiral stirrup reinforcement were tested; these configurations had a noticeable impact on the wide beams as the shear capacity and the ductility had highly improved [9].

Another approach was introduced by using internal and external fasteners on thirteen wide beam specimens; the mode of failure and the shear capacity were improved [10]. In 2023, five shallow beams with ultra-high-performance fiber-reinforced concrete were tested with different spacings, and the area of the stirrups was considered both variables. They were tested under torsion, but no notable impact was observed [11]. The advancements in the field of artificial intelligence and machine learning in recent years have opened a lot of research opportunities regarding the behavior of the different concrete elements. Implementing and using several experimental and finite element studies, the shear capacity of the reinforced concrete beams was predicted via machine learning in different recent studies [12–14]. Using the same techniques, the mode of failure of the reinforced concrete beams can also be predicted [15]. After carefully studying the previous research and investigations, several gaps in these studies were identified and considered for this experimental investigation [16]. Previous experimental studies had only considered one aspect ratio (b/d) per study, meaning that all the specimens in the same study had the same cross section and only steel configurations or types of loading were changed during testing. Concrete characteristic strength (Fc') was another parameter that was mostly ignored during experimental studies, as the researchers were focused on the percentage and the type of steel configurations. Compression steel and its ratio ($\rho' = As'/bd$) in wide beams were never considered in recent studies; its effect on the shear capacity and the behavior of the wide-shallow beams is yet to be considered.

2. Objectives

The objective of this research is to experimentally investigate the effect of three parameters on the shear capacity of shallow-wide RC beams. The considered parameters were the aspect ratio (width to depth ratio b/d), the concrete compressive strength (Fc'), and the ratio of the compression steel rebars to the concrete section ($\rho' = As'/bd$). Test results were discussed in terms of failure mode, first crack, shear capacity, beam stiffness, and ductility. Also, they are used to assess the theoretical design values of six different design codes and design guidelines. Moreover, a comparison between the experimental results and predicted values using the GP and EPR methods was made. The methodology of this research is illustrated in Figure 1.
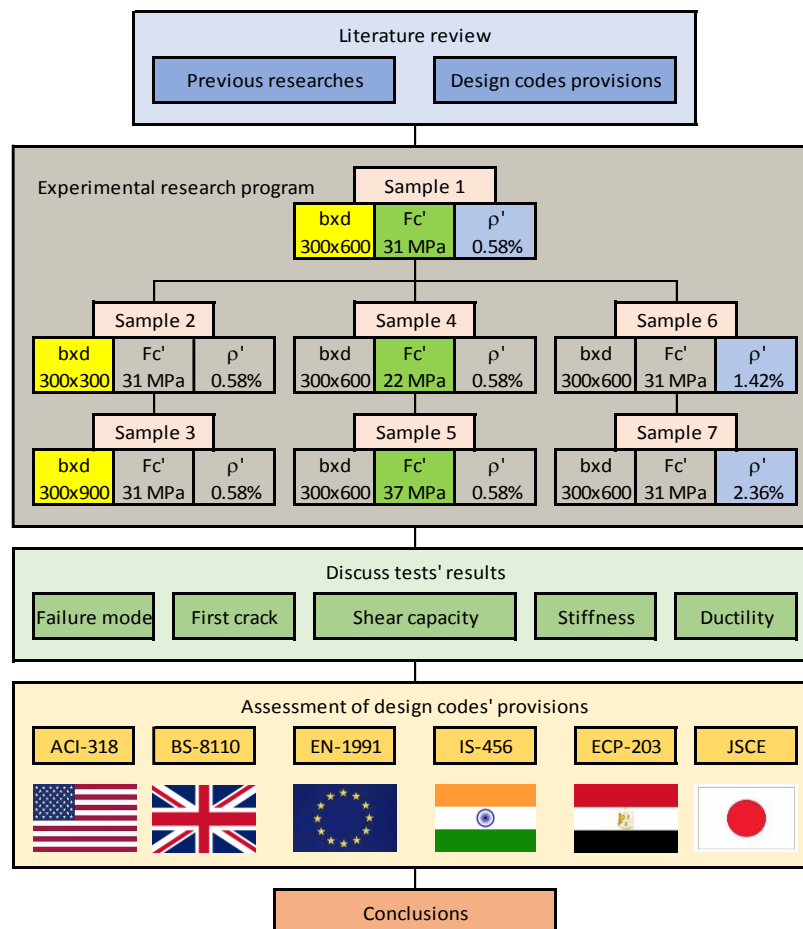

Figure 1. The research methodology

3. Experimental Work

3.1. Samples Configurations and Materials

The conducted experimental program included seven shallow beam specimens. All beams had the same length (1200 mm), span (1050 mm), thickness (200 mm), longitudinal tension rebar ratio (ρ = As/bd = 2.83%), stirrup spacing (S = 100 mm), and shear reinforcement ratio (ρsh = Ash/b.S = 0.33%). High-tensile steel (40/60, Fy = 416 MPa) was used for longitudinal rebars (denoted as "T"), and mild steel (24/37, Fy = 233 MPa) was used for stirrups (denoted as "R"). Three cylinders (Dia. 150 x 300 mm) were cast for each concrete mix and tested just before testing the beams to evaluate the characteristic strength (Fc') as shown in Table 1, with the grading curve for the coarse and fine aggregates used shown in Figure 2. Also, three samples of each steel type and diameter were tested in tension to determine their yield strengths (Fy), as mentioned above and shown in Table 2.

Table 1. Concrete mixes and characteristic strength after 28 days

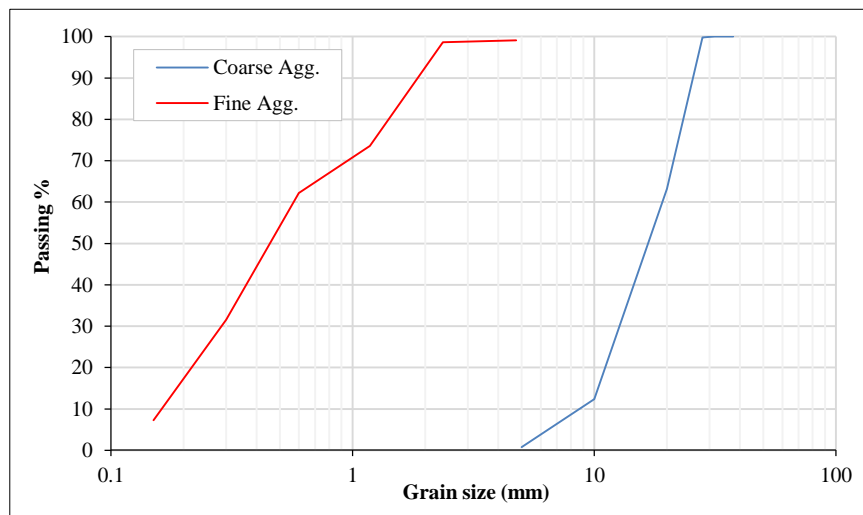| Concrete Mix	Fc' (MPa)	Slump (mm)	Cement (kg/m³)	Water (kg/m³)	Coarse Agg. (kg/m³)	Fine Agg. (kg/m³)	Plasticizer (kg/m³)
1	31	200	450	200	1040	640	6
2	22	200	400	225	1040	630	-
3	37	200	500	195	1040	625	9

Figure 2. Grading curve for the coarse and fine aggregates used in the concrete mixes

Table 2. Details of the steel bars used of longitudinal reinforcement and stirrups

Steel type	Grade	Tested yield strength
High tensile steel	400/600	416 MPa
Mild steel	240/370	233 MPa

The tested beams were placed in three groups (group for each considered parameter). Each group contained three beams (including the common control beam B1). The first group (B1, B2, B3) had addressed the aspect ratio (b/d = 3.3, 1.67, 5), the second one (B1, B4, B5) had addressed the concrete characteristic strength (Fc' = 31, 22, 37 MPa), and the last one (B1, B6, B7) had addressed the compression steel ratio (ρ'=As'/bd = 0.58, 1.42, 2.36%). Table 3 summarizes the configurations of each beam.

Table 3. Summary for the configurations of each tested beam

Beam	b × d (mm)	Cross section	Stirrups (ρsh=Ash/bS)	Tension rebars (ρ=As/bd)	Compression rebars (ρ'=As'/bd)	Char. Strength (Fc') (MPa)
B1	600×200		4R8-100 (0.33%)	12T18 (2.83%)	8T10 (0.58%)	31
B2	300×200		2R8-100 (0.33%)	6T18 (2.83%)	4T10 (0.58%)	31
B3	900×200		6R8-100 (0.33%)	18T18 (2.83%)	12T10 (0.58%)	31

B4	600×200		4R8-100 (0.33%)	12T18 (2.83%)	8T10 (0.58%)	22
B5	600×200		4R8-100 (0.33%)	12T18 (2.83%)	8T10 (0.58%)	37
B6	600×200		4R8-100 (0.33%)	12T18 (2.83%)	6T18 (1.42%)	31
B7	600×200		4R8-100 (0.33%)	12T18 (2.83%)	10T18 (2.36%)	31

3.2. Test Setup and Samples Instrumentation

All beams were tested up to failure under a monotonic load using a three-point bending test. All samples (beams, cylinders, and steel samples) were tested in a concrete laboratory in El Shorouk Academy, El Shorouk City, Egypt. The lab is equipped with a testing frame containing a 1000 KN hydraulic jack, as shown in Figure 3-b. The tested beams were placed in the testing frame, and two cylindrical steel bars acted as supports; one was welded to a base plate to simulate a hinged support, and the other steel bar was free to act as a roller support. The midpoint of the tested specimens was aligned below the hydraulic jack, and the load was transferred from the jack to the beam through a distrusting steel beam to convert the point load of the jack to a line load on the beam. The test setup is presented in Figure 3-a.
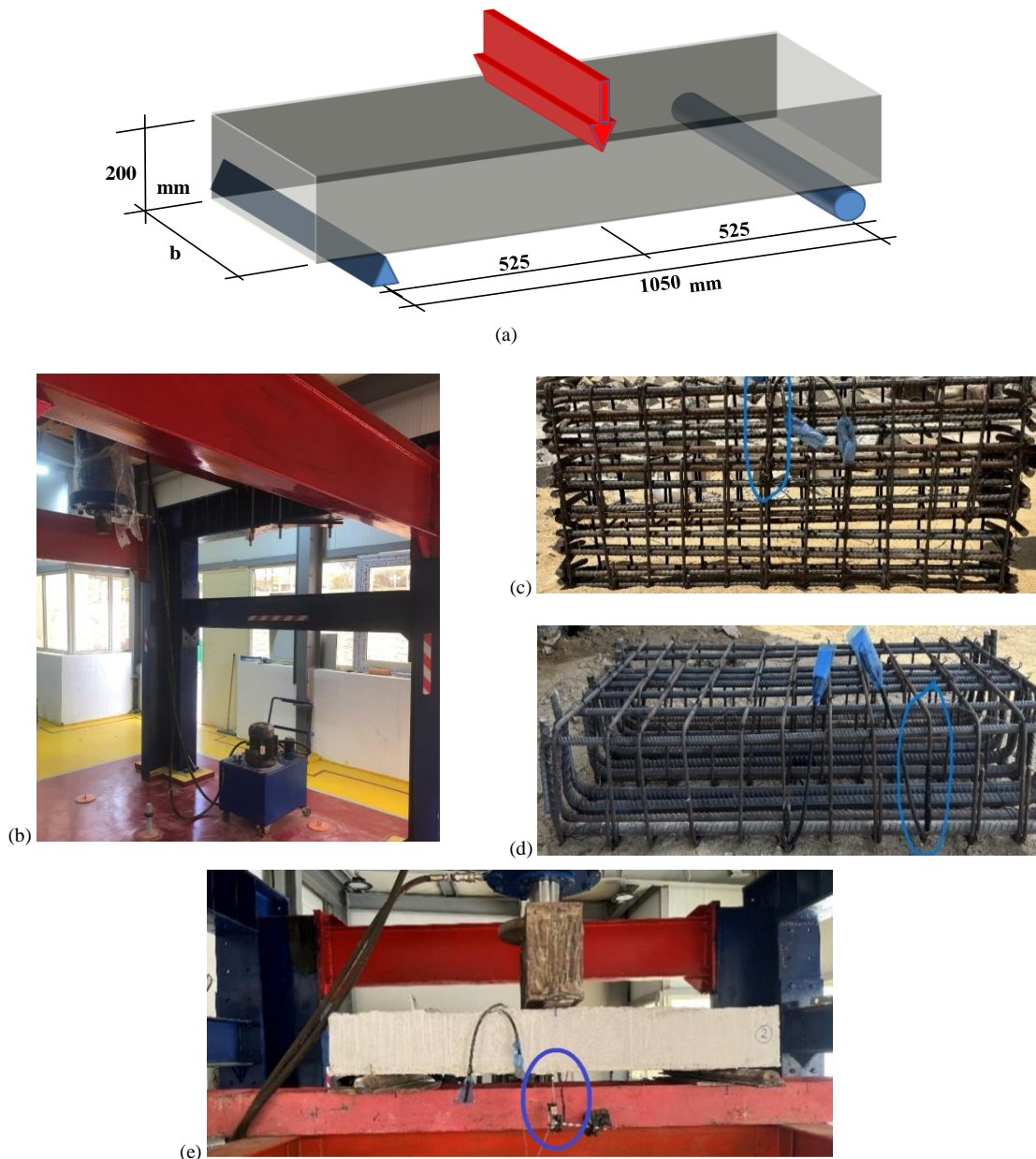

(a)

(b)

(c)

(d)

(e)

Figure 3. Samples instrumentation & test configurations, a) test setup, b) testing frame, c) longitudinal rebars strain gauge, d) stirrups strain gauge, e) LVTDs locations

Each tested beam was provided by two strain gauges, one at the midpoint of the middle longitudinal tension rebar and the other on the outer branch of the stirrup at (d/2 ≈100 mm) from the support. The first one was used to detect the flexural failure mode, while the second one was used to detect the shear failure mode. Besides these two gauges, the mid-span deflection was measured using two LVTD's below the beam at the front and back sides. Finally, the testing load was measured by a load cell attached to the hydraulic jack. All measurements were automatically recorded during the test by a data acquisition system. Figures 3-c to 3-e illustrate the location of the strain gauges and LVTD's.

4. Test Results

Applied load, mid-span deflection, and strain in both ties and tension rebars were automatically recorded using the data acquisition system for all the tested wide-shallow beam specimens. In addition, crack patterns, locations, orientations, and propagation were visually observed and drawn on the sample. The beams were tested under strain-controlled loading at a rate of 1.0 mm/min. The first flexural crack at the lower surface of the beam was observed, and the corresponding load and deflection were recorded. The applied load gradually increased until failure.

Figure 4 shows the recorded load-deflection curves up to the failure loads (maximum loads), while Table 4 summarizes the recorded values of load and deflection at the first crack and ultimate stage, besides the ultimate strains in ties and tension rebars. The last column in the table shows photographs of the crack pattern.
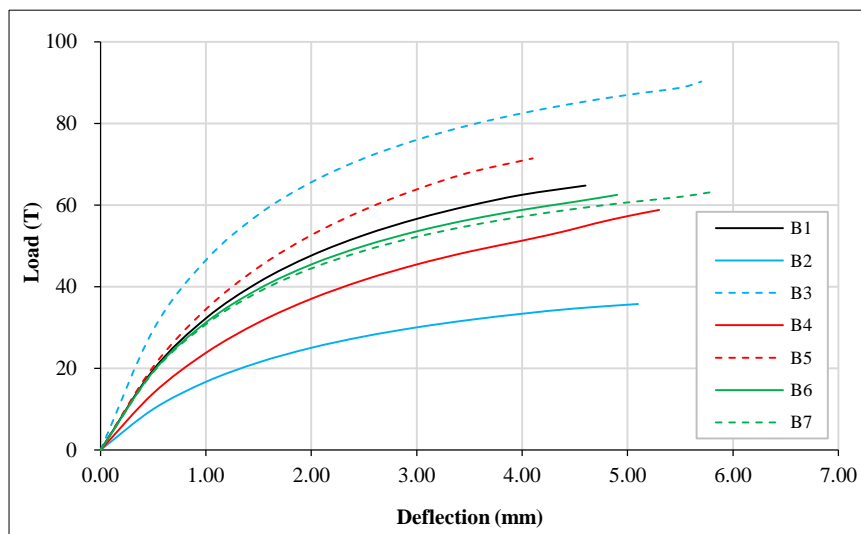

Figure 4. Load-deflection curves for tested beams

Table 4. Summary for the experimental results showing the loads, deflection (cracking and ultimate) and the strain in ties and longitudinal reinforcements

Beam	$P_{cr\ exp}$ (kN)	$P_{u\ exp}$ (kN)	Δ_{cr} (mm)	Δ_{u} (mm)	ε_{tie} (με)	ε_{ten} (με)	Crack pattern
B1	92	648	0.22	4.60	1810	1415	
B2	49	357	0.25	5.10	2065	1580	
B3	142	903	0.25	5.70	2445	1855	
B4	77	588	0.24	5.30	2410	1830	
B5	102	714	0.20	4.10	1630	1270	

B6	91	663	0.20	4.90	1820	1445	
B7	93	687	0.20	5.80	2350	1880	

5. Discussion

5.1. Mode of Failure

All the tested beams showed almost the same behavior. Vertical flexural cracks started on the lower surface of beams at mid-span; the number and width of these cracks were increased while applying the load. At a certain stage, diagonal cracks connecting the loading point and the supporting points appeared and increased in length and width until failure, as shown in Table 4. All observed failures were ductile and gradual, without sudden changes, as illustrated in Figure 4. The visual observations indicated that all the beams had failed due to shear. The listed maximum strain values in Table 4 showed that the strain in the tension rebars was less than their yield strain ($\varepsilon y = Fy/Es = 416/200\,000 = 2080$ μ-strain), which means that the specimens did not fail due to bending. On the other hand, the strain values in the ties exceeded the yield strain ($\varepsilon y = Fy/Es = 233/200\,000 = 1165$ μ-strain), which means that all the specimens had failed due to shear.

5.2. First Crack Load

The recorded first crack loads of the tested wide-shallow beams are listed in Table 4. It had mainly depended on the beam section, the tensile strength of concrete, and slightly on the reinforcement ratio; hence, it made perfect sense that the first crack loads of beams (B1, B6, B7) were almost the same (92, 91, 93 kN) as they had the same beam cross section and concrete strength. Also, it was expected that the first crack loads of the beams (B1, B2, and B3) would be proportional to their widths (92, 49, and 142 kN) since they all have the same depth and concrete strength but widths of 600, 300, and 900 mm, respectively. Finally, increasing the compressive strength of concrete had enhanced its tensile strength ($Ft = 0.6\sqrt{Fc'}$), the first crack load of B1 (92 kN) should be greater than the one of B4 (77 kN) and less than the one of B5 (102 kN). Figure 5 compares both experimental and theoretical values of the first crack load of all tested beams.
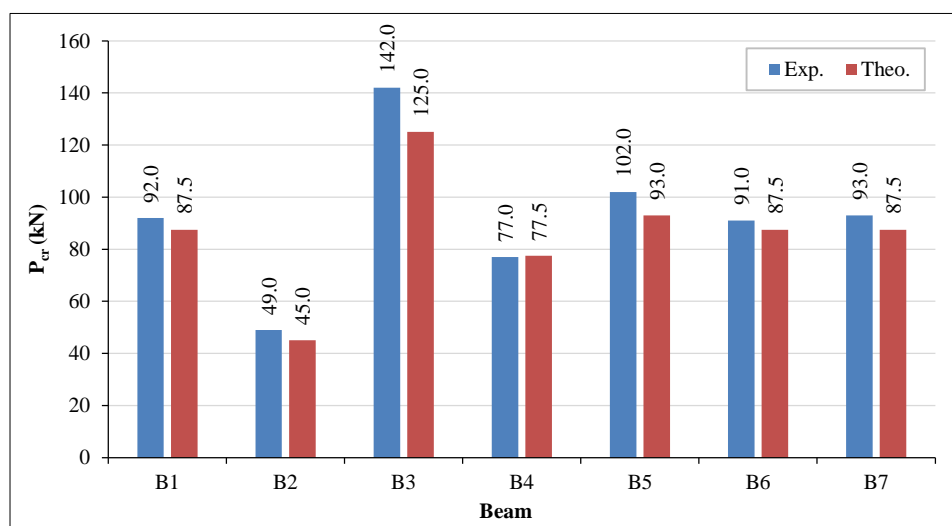

Figure 5. Experimental and theoretical first crack load values of tested beams, (kN)

5.3. Shear Capacity

The experimental shear capacities of the tested wide-shallow beams specimens are to equal half the recorded ultimate loads listed in Table 4. Revising these values indicated the following:

- Comparing the shear capacities of beams (B1, B2, and B3) (324, 179, and 452 kN, respectively) showed that although the shear reinforcement ratio ($\rho sh = Ash/b.S = 0.33\%$) is constant, the ultimate shear stress ($qu = Vu/bd$) decreased linearly with increasing the aspect ratio (b/d) (3.00, 3.31, and 2.79 MPa, respectively), as shown in Figures 6-a. This was due to the size effect; similar reductions in shear capacity with increasing depth (d) are implemented in many design codes, such as BS-8110 [17], EN-1992 [18], IS-456 [19], and JSCE [20], as shown in Figure 7.
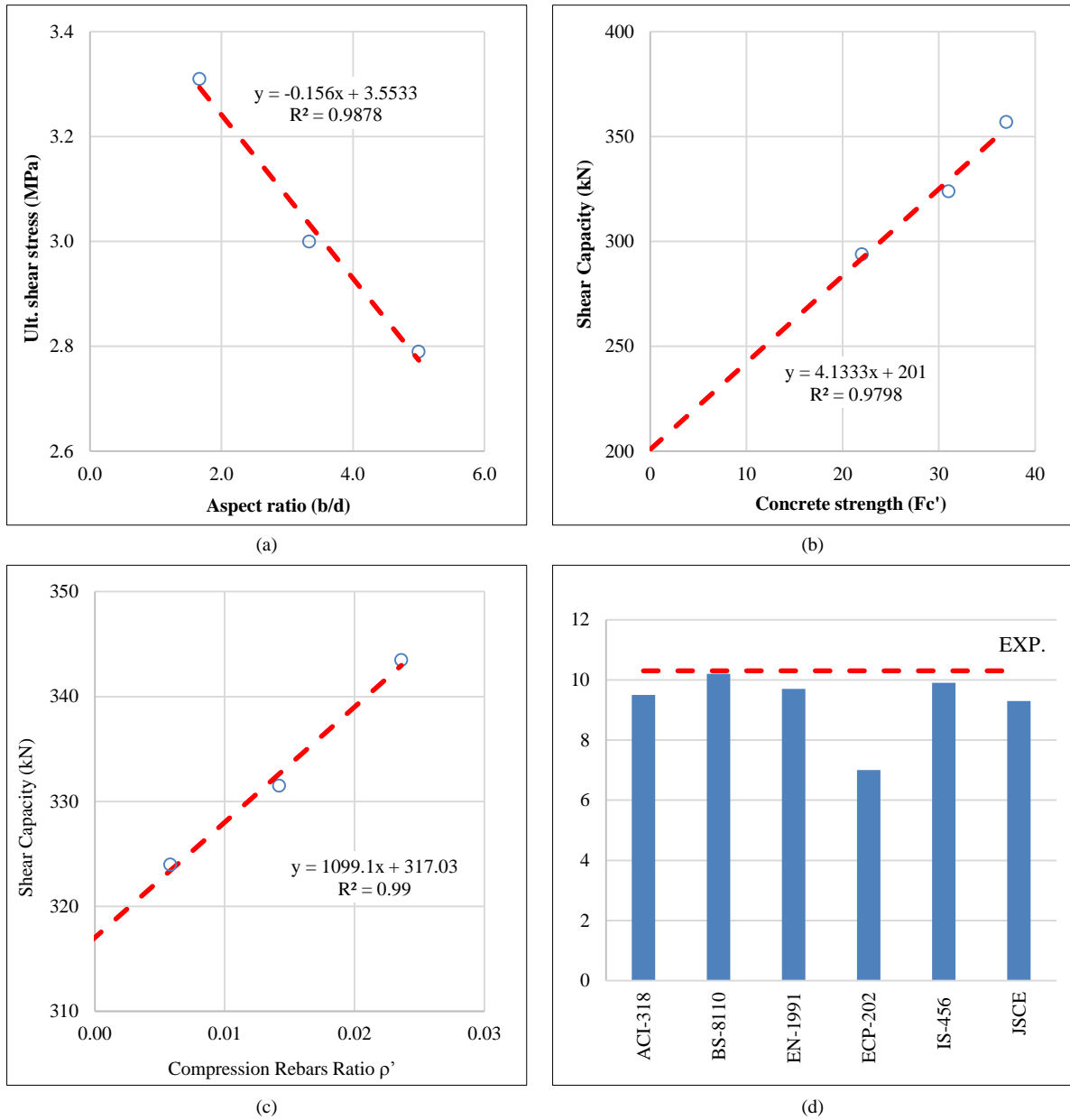
(a)

(b)

(c)

(d)

Figure 6. Analysis of test results, a) Ultimate shear stress vs. aspect ratio, b) Shear capacity vs. concrete strength, c) shear capacity vs. compression rebars ratio and d) Experimental shear stress in compression rebars vs. code provisions

Code	Ultimate Shear strength of Concrete $q_c = (V_c / b.d)$
ACI-318	$0.16 (Fc')^{0.5} + 17 \rho$
BS-8110	$0.79 (100 \rho)^{0.33} (400/d)^{0.25} (Fcu/25)^{0.33}$
EN-1991	$0.18 [1+(200/d)]^{0.5} (100 \rho Fc')^{0.33}$
IS-456	$1.5 q_c$ (from table)
ECP-203	$0.16 (Fcu)^{0.5}$
JSCE	$0.2 (1000/d)^{0.25} (1000 \rho)^{0.33} (Fc')^{0.33}$

(Fc', Fcu) are the characteristics strength of concrete cylinder and cube respectively, (d) is the beam depth, ($\rho= As/b.d$) is the longitudinal tension rebars ratio. All unis are in (N, mm).

Figure 7. Design codes formulas for the ultimate shear capacity of concrete

- Generally, the shear capacity of a RC beam (Vu) is mainly the summation of the shear capacity endured by the concrete cross-section (Vc), the shear capacity contributed by the shear reinforcement (stirrups) (Vs) and the compression rebars contribution (Vρ'). Equation 1 presents the basic formula to estimate the shear capacity of RC beam.

$$Vu = Vc + Vs + V\rho' = (qc.b.d) + (Ash.Fyt) + (q_{\rho'}.As') \qquad (1)$$

where (qc) is the ultimate concrete shear strength, (b & d) are beam width and depth, (Ash) is the cross-sectional area of all stirrups intersected by the shear crack, (Fyt) is the yield stress of stirrups, (qρ') is the shear stress in the compression rebars and (As') is compression rebars area.

Equation 1 was used to distinguish both concrete and reinforcement contributions of beams (B1, B4, B5). These beams are identical but their concrete characteristic strength (Fc') were different, hence, their shear reinforcement and compression rebars contributions (Vs+Vρ') are the same and equal to 201 kN as shown on Figure 6-b (the capacity at Fc'=0). Accordingly, the ultimate concrete shear strengths (qc) of these beams are (1.14, 0.86, 1.44 MPa) respectively. Table 5 presents a comparison between experimental (qc) values and design codes provisions.

Table 5. Comparison between experimental (qc) values and design codes provisions

Beam	Fc' (MPa)	qc (MPa)						
		Exp.	ACI-318	BS-8110	EN-1992	ECP-203	IS-456	JSCE
B4	22	0.86	1.23	1.41	1.04	0.84	1.29	1.26
		100%	143%	163%	120%	97%	150%	146%
B1	31	1.14	1.37	1.58	1.16	1.00	1.43	1.41
		100%	120%	139%	102%	87%	125%	124%
B5	37	1.44	1.48	1.70	1.25	1.12	1.47	1.52
		100%	102%	118%	87%	77%	102%	106%

- Specimens (B1, B6, B7) had the same tension longitudinal reinforcement and shear reinforcement but the compression reinforcement ratio (ρ') was changed through the three specimens from 0.58 % to 1.42 % and 2.36 % respectively. Since they all have the same section and shear reinforcement, their shear capacities (324, 336, 347 kN respectively) had indicated that there is a slight enhancement in shear capacity with increasing the compression rebars ratio (ρ'). This enhancement was linear as presented in Figure 6-c, and hence, it is expected that the shear capacity of beam without compression rebars is 317 KN and the rest is the contribution of the compression rebars, the shear stress in the compression rebars (qρ' = (Vu-317) /As') was 10.3 MPa. This enhancement was not due to friction shear (dowel action) since the rebars were under compression; also, the shear stress in the rebars is almost eight times the concrete shear strength. Hence, it was concluded that the compression rebars acted as an additional virtual concrete area equals to the shear modular ratio (Gs/Gc) multiplied by the compression rebars area as shown in Equation 2, where (Gs & Gc) are the modulus of rigidity of steel and concrete respectively.

$$\frac{V_{\rho'}}{As'} = \frac{V_u - 317}{As'} = q_{\rho'} = q_c \frac{Gs}{Gc} \qquad (2)$$

Considering Fc'= 31 MPa, Ec = 26 GPa, νc=0.16, Es = 200 GPa, νs=0.30, hence, Gs/Gc = 7.0 and (qρ') equals to 9.5, 10.2, 9.7, 7.0, 9.9 and 9.3 MPa using ACI-318, BS-8110, EN-1991, ECP-202, IS-456 and JSCE respectively. Figure 6-d compares the experimental value of (qρ') with design codes provisions.

- Based on the previous two points, the contribution of the shear reinforcement (Vs) alone could be estimated as (201- qρ'. As'), for (qρ' = 10.3 MPa), (As' = 8T10), hence, Vs = 194.5 KN. Theoretically, (Vs =Ash · Fyt), For (Ash = 4 stirrups dia. 8 mm, 4 branches = 800 mm2) and (Fyt=233 MPa), hence, Vs should be 186.4 KN which is about 96 % of the estimated one.

- Finally, Table 6 compares the experimental total shear capacity (Vu) with the calculated values form different design codes.

Table 6. Total shear capacity obtained from the exp. program vs. code provisions

	Total shear capacity (Vu) in kN						
	B1	B2	B3	B4	B5	B6	B7
Exp.	324	179	452	294	357	332	344
BS-8110	374	177	525	352	385	374	374
ACI-318	387	183	544	371	396	387	387
EN-1992	392	185	551	369	403	392	392
ECP-203	325	162	488	307	334	325	325
JSCE	359	170	507	340	368	359	359
IS-456	373	186	559	373	373	366	378

5.4. Load-Deflection Curve

The method for calculating ductility and the dissipated energy for the load deflection curve used for this investigation was prioritized and simplified by Ramadan et al. [21]. Figure 4 summarizes the load-deflection curves of the seven tested beams. Analyzing the load-deflection curve included the 1st crack load and its corresponding deflection (initial or un-cracked stiffness), the ultimate load and its corresponding deflection (where the ultimate load is twice the shear capacity), identifying the failure type (smooth or sudden), calculating the ductility, and estimating the dissipated energy. Figure 8 illustrates the definitions of these terms. Table 7 summarizes the analysis results of the seven load-deflection curves, and Figure 9 presents them graphically.
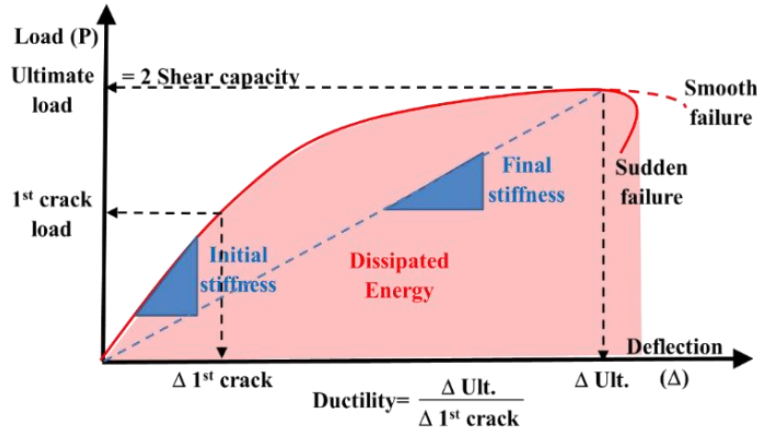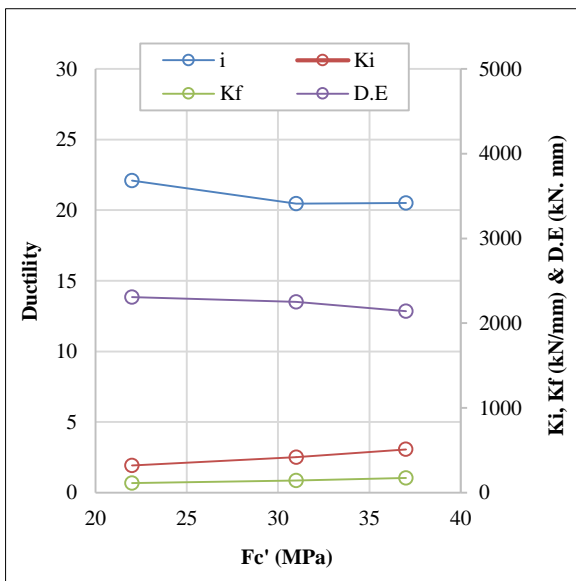

Figure 8. Analyzing the load-deflection curve

Table 7. Summary for load-deflection curves analysis

Beam	Ki kN/mm	Kf kN/mm	D.E. kN.mm	Ductility
B1	418	141	2249	20.9
B2	196	70	1368	20.4
B3	568	158	4477	22.8
B4	321	111	2309	22.1
B5	510	174	2142	20.5
B6	455	135	2334	24.5
B7	465	118	2882	29.0

Ki: initial stiffness, Kf: final stiffness, D.E: Dissipated Energy.

(a)   (b)

(c)
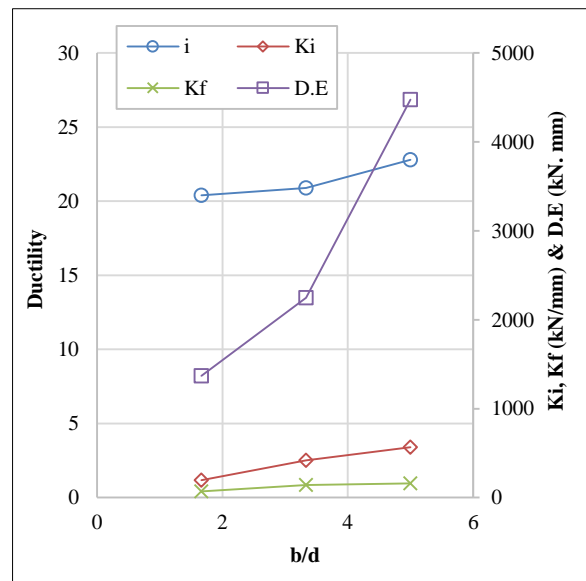
Figure 9. Analyzing the load-deflection curve
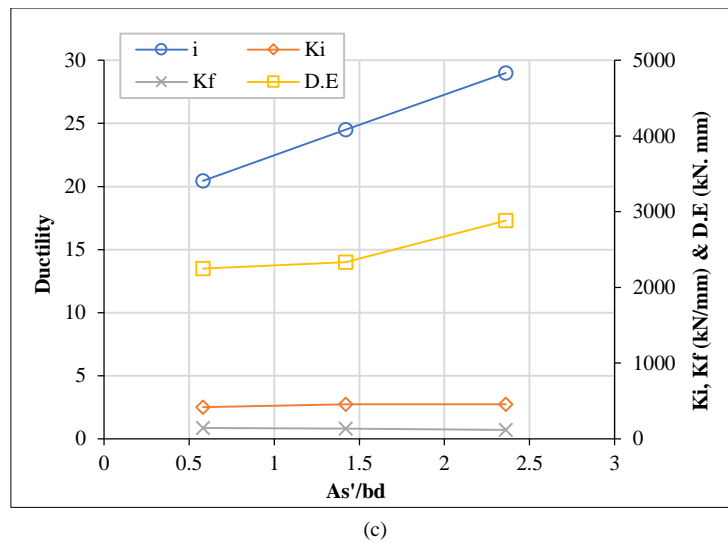
The influence of concrete strength (Fc') on the beam behavior is presented in Figure 9-a. It indicates that both initial and final stiffnesses are enhanced with increasing the (Fc'), which was expected due to the enhancement of the elastic modulus of concrete. On the other hand, both ductility and dissipated energy were slightly decreased with increasing the (Fc'). As the concrete gets stronger, it gets stiffer (initially and finally) than the weaker concrete, and since its deflection is smaller, as shown in Table 4, the (Δu) values are 5.30, 4.60, and 4.10 mm for (Fc') values of 22, 31, and 39 MPa, respectively. Hence, increasing the load while reducing the deformations keeps the area under the curve (dissipated energy) almost constant. Also, reducing both cracked and ultimate deflections keeps the ductility almost constant too.

Regarding the effect of the aspect ratio (b/d), Figure 9-b indicated that both initial and final stiffnesses are improved by increasing the (b/d); this is due to increasing the beam section (since the depth is constant). Similarly, the increase in the DE was due to the increase in the ultimate load and, accordingly, the area below the curve. And finally, the ductility was almost constant because both cracking and ultimate deflection values improved with increasing the beam section.

Finally, the impact of the compression rebar ratio (ρ') is presented in Figure 9-c. It had a very slight impact on the stiffness since it had an insignificant contribution to the beam inertia. Besides that, the minor contribution of compression rebars in the shear capacity had made the load-deflection curves of beams (B1, B6, B7) so close, and hence they almost had the same area below the curve (DE). In contrast, the chart shows a significant improvement in ductility with increasing (ρ') because the three beams have the same cracking deflections, but the ultimate deflection increases with increasing the compression rebars.

6. Comparison with Earlier Researches

The experimented results presented in this paper were compared to two developed equations: the first equation was developed using genetic programming techniques (GP) and the second equation using evolutionary polynomial regression (EPR). Both previously mentioned equations were developed for the purpose of predicting the shear capacity of RC beams and are shown in Table 8. The GP equation was developed in 2021 using a dataset of 553 tests [22], while the EPR equation was developed in 2022 using a dataset of 1500 tests with an accuracy of 76.5% [23].

Table 8. Shear capacity formulas from previous research

Ref.	Formula
[22]	$Vu = \dfrac{1.25 \, Ln\,(1.3 + 0.7\mu_{sh}.\,fys\ + 0.2.\,\rho)}{Ln\,(45(a/d)(Ec/Es))} \cdot b.\,d.\,\sqrt{fc'}$
[23]	$Vu = \dfrac{d(64\,\rho - 24d + 6.8) - a(234b.\,\rho + 1) - 0.11}{b.\,d} + \dfrac{154a - 1080d + 66.5}{d.\,fc'} + \dfrac{a}{1.75d^2} + \dfrac{d(694\,d + 370\,b - 1317\,\rho) - 11}{a}$ $-\dfrac{b}{2.75\rho} - \dfrac{fc'^2}{580} + 128\,b^2 - 78.5\,d^2 + 31.9\,a + 19\rho\,(360\,b + 150\,d + fc' - 950\,\rho) - 22.5$

Vu: Total shear capacity, μ_{sh}: Shear reinforcement ratio, Fys: Yield strength of shear reinforcement steel, ρ: Longitudinal reinforcement ratio, a: Shear span of the beams, d: Depth of the beams, Fc': Concrete characteristic strength, Ec: Modulus of elasticity of concrete, Es: Modulus of elasticity of steel reinforcement.

The values of the shear capacities for the tested seven wide-shallow beam specimens were calculated from the GP and the EPR equations, as shown in Table 9. Also, a comparison between the predicted values and the experimental values was made. The accuracy of the GP technique was low compared to the EPR method, as it ranged from 65% to 78%.

Table 9. The calculated values from the (GP) and the (EPR) equations and their accuracies

Specimen	Vu Exp (kN)	Vu (GP) (kN)	$\dfrac{Vu\,GP}{Vu\,Exp}$	Vu (EPR) (kN)	$\dfrac{Vu\,(EPR)}{Vu\,Exp}$
B1	324	234	0.72	272	0.84
B2	179	117	0.65	109	0.61
B3	452	351	0.78	374	0.83
B4	294	209	0.71	262	0.89
B5	357	248	0.69	276	0.77
B6	332	234	0.70	272	0.82
B7	344	234	0.68	272	0.79

Meanwhile, the accuracy of the EPR technique was between 77% to 89%, except for B2, which had the lowest accuracy of 61%. (B2) had an aspect ratio of 1.67, meaning that with an aspect ratio of 3.3 and above, the predicted values of the EPR technique were the most accurate.

A relationship between the experimental values of the shear capacities and the predicted results had been constructed for both the GP and EPR methods. The accuracy of the GP method was 72%, as per the equation shown in Figure 10-a. Moreover, the accuracy of the EPR method was a little above 81%, as shown in Figure 10-b.

(a) (b)
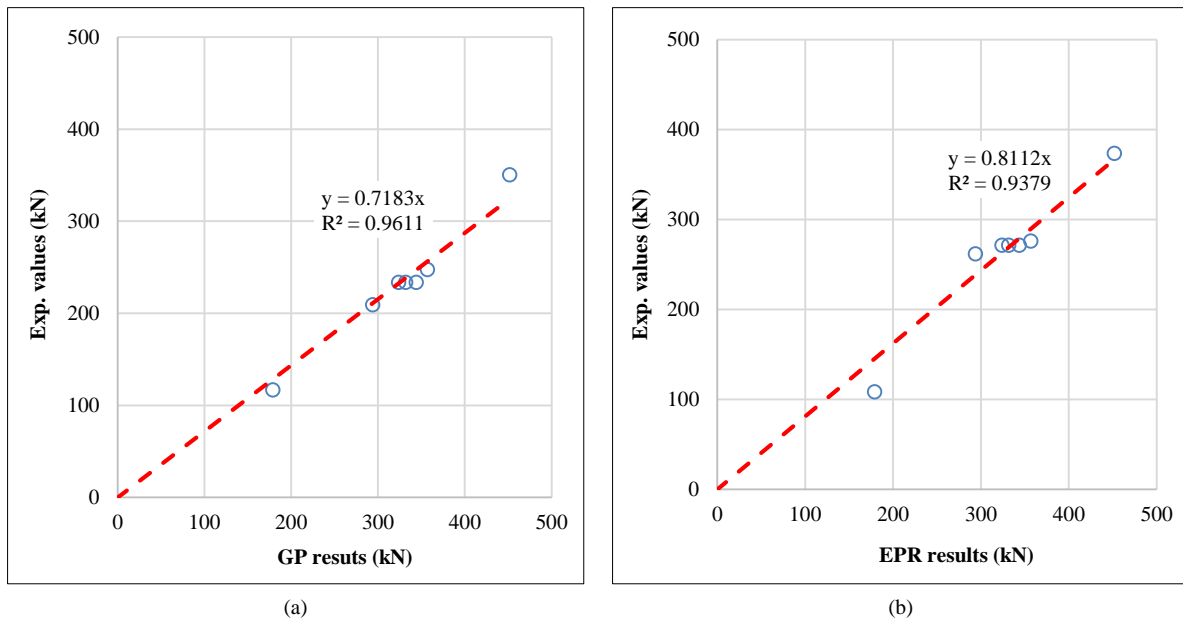
Figure 10. Relation between the predicted (Vu) values and the experimental results

7. Conclusions

This research experimentally investigated the impact of aspect ratio, characteristic strength of the concrete, and compression rebars on the shear capacity of wide-shallow RC beams. Seven shallow beams were tested up to failure using a three-point monotonic bending test setup; the results were recorded, analyzed, and compared with the provisions of six different design codes. The outcomes of this research could be summarized as follows:

- Changing the aspect ratio of the beams (width/depth) showed that increasing the aspect ratio from 1.66 to 5.00 had decreased the ultimate shear strength of the beam from 3.30 to 2.79 MPa. This reduction may be due to the size effect because the width increased from 300 to 900 mm while the depth was kept constant at 180 mm.

- The estimated experimental shear contribution of concrete increased from 0.86 to 1.44 MPa by increasing the characteristic strength from 22 to 37 MPa. The recommended concrete shear strength in different codes ranged between 77% and 163% of the experimental values. ECP-203 was the most conservative one due to neglecting the effect of the longitudinal tension rebars; BS-8110 was the least conservative code; and EN-1992 was the closest one to the experimental results.

- Compression rebars had a minor impact on the shear capacity of the beams (2.5% to 9.5%) compared to the rebar ratio of 0.58% to 2.36%. The analysis results showed that compression rebars acted as additional virtual concrete area with a shear modular ratio of (Gs/Gc).

- Although all design codes neglected the shear reinforcement contribution, the analyzed results showed that the shear reinforcement was fully functional up to yield, and its contribution was about 55 to 60% of the shear capacity.

- Both the initial and final stiffness increased with increasing the concrete section (or aspect ratio) and the elastic modulus (or characteristic strength), but they were not significantly affected by the compression rebar ratio.

- The dissipated energy was mainly affected by the beam size (or aspect ratio), while the ductility was mainly affected by the compression rebar ratio.

- Comparing the experimental results with two AI predictive models from previous research showed that the calculated shear capacities of both the GP model and the EPR model are about 72% and 81% of the experimental ones, respectively.

8. Declarations

8.1. Author Contributions

Conceptualization, A.S. and A.E.; methodology, A.S.; validation, A.S. and A.E.; formal analysis, A.S.; investigation, A.S.; resources, A.S.; data curation, A.E.; writing—original draft preparation, A.S.; writing—review and editing, D.M.; visualization, D.M.; supervision, A.K.; project administration, A.K.; funding acquisition, A.S. All authors have read and agreed to the published version of the manuscript.

8.2. Data Availability Statement

The data presented in this study are available on request from the corresponding author.

8.3. Funding

The authors received no financial support for the research, authorship, and/or publication of this article.

8.4. Conflicts of Interest

The authors declare no conflict of interest.

9. References

[1] Sherwood, E. G., Lubell, A. S., Bentz, E. C., & Collins, M. P. (2007). One-way shear strength of thick slabs and wide beams. ACI Structural Journal, 104(5), 640–641. doi:10.14359/18229.

[2] Serna-Ros, P., Fernandez-Prada, M. A., Miguel-Sosa, P., & Debb, O. A. R. (2002). Influence of stirrup distribution and support width on the shear strength of reinforced concrete wide beams. Magazine of Concrete Research, 54(3), 181–191. doi:10.1680/macr.2002.54.3.181.

[3] ACI 318-19. (2019). Building Code Requirements for Structural Concrete (ACI 318-19) Commentary on Building Code Requirements for Structural Concrete (ACI 318R-19). American Concrete Institute (ACI), Michigan, United States.

[4] Lubell, A., Sherwood, T., Bentz, E., & Collins, M. (2004). Safe shear design of large wide beams. Concrete International, 26(1), 66-78.

[5] Özbek, E., Aykaç, B., Bocek, M., Yılmaz, M. C., Mohammed, A. B. K., Er, Ş. B., & Aykaç, S. (2020). Behavior and strength of hidden RC beams embedded in slabs. Journal of Building Engineering, 29. doi:10.1016/j.jobe.2019.101130.

[6] Alluqmani, A. E. (2020). Effect of the transversal-spacing of stirrup-legs on the behavior and strength of shallow concealed RC beams. Journal of Engineering, Design and Technology, 19(4), 932–942. doi:10.1108/JEDT-06-2020-0224.

[7] Taha, M. G., & Abbas, A. L. (2021). Effect of Longitudinal Maximum Spacing of Shear Reinforcement for wide Reinforced Concrete Beams. IOP Conference Series: Materials Science and Engineering, 1076(1), 012118. doi:10.1088/1757-899x/1076/1/012118.

[8] Mahmoud, S. M., Mabrouk, R. T. S., & Kassem, M. E. (2021). Behavior of RC Wide Beams under Eccentric Loading. Civil Engineering Journal, 7(11), 1880–1897. doi:10.28991/cej-2021-03091766.

[9] Elansary, A. A., Elnazlawy, Y. Y., & Abdalla, H. A. (2022). Shear behaviour of concrete wide beams with spiral lateral reinforcement. Australian Journal of Civil Engineering, 20(1), 174–194. doi:10.1080/14488353.2021.1942405.

[10] Moubarak, A. M. R., Elwardany, H., Abu El-hassan, K., & El-Din Taher, S. (2022). Shear strengthening of wide-shallow beams by inserted fasteners. Engineering Structures, 268. doi:10.1016/j.engstruct.2022.114554.

[11] Yousef, A. M., Marami, N. A., & Tahwia, A. M. (2023). Experimental and Numerical Investigation for Torsional Behavior of UHPFRC Shallow and Deep Beams. Arabian Journal for Science and Engineering, 1–14. doi:10.1007/s13369-023-07701-3.

[12] Koo, S., Shin, D., & Kim, C. (2021). Application of principal component analysis approach to predict shear strength of reinforced concrete beams with stirrups. Materials, 14(13), 3471. doi:10.3390/ma14133471.

[13] Fan, X., Wang, S., & Zhang, Z. (2020). A Study of Size Effect in Shear Resistance of Reinforced Concrete Beams Based on Machine Learning. IOP Conference Series: Earth and Environmental Science, 455(1), 12099. doi:10.1088/1755-1315/455/1/012099.

[14] De Domenico, D., Quaranta, G., Zeng, Q., & Monti, G. (2022). Machine-learning-enhanced variable-angle truss model to predict the shear capacity of RC elements with transverse reinforcement. Procedia Structural Integrity, 44, 1688–1695. doi:10.1016/j.prostr.2023.01.216.

[15] Wang, S., Ma, C., Wang, W., Hou, X., Xiao, X., Zhang, Z., Liu, X., & Liao, J. J. (2023). Prediction of Failure Modes and Minimum Characteristic Value of Transverse Reinforcement of RC Beams Based on Interpretable Machine Learning. Buildings, 13(2), 469. doi:10.3390/buildings13020469.

[16] Soliman, A. A., Mansour, D. M., Ebid, A., & Khalil, A. H. (2023). Shallow and Wide RC Beams, Definition, Capacity and Structural Behavior – Gap Study. The Open Civil Engineering Journal, 17(1), 1-11. doi:10.2174/18741495-v17-e230725-2023-28.

[17] BS 8110-1:1997. (1997). Structural use of concrete. Code of practice for design and construction (AMD 9882- 13468). British Standards Institution (BSI), London, United Kingdom.

[18] EN 1992-1-1. (2004). Eurocode 2: Design of concrete structures - Part 1-1: General rules and rules for buildings. European Committee for Standardization (CEN), Brussels, Belgium.

[19] IS 456. (2000). Plain and Reinforced Concrete-Code of Practice (Fourth Revision). Bureau of Indian Standards, New Delhi, India.

[20] JSCE Guidelines for Concrete No. 16. (2007). Standard Specifications for Concrete Structures. Japan Society of Civil Engineers, Tokyo, Japan.

[21] Ramadan, M., Ors, D. M., Farghal, A. M., Afifi, A., Zaher, A. H., & Ebid, A. M. (2023). Punching shear behavior of HSC & UHPC post tensioned flat slabs – An experimental study. Results in Engineering, 17, 100882. doi:10.1016/j.rineng.2023.100882.

[22] Ebid, A. M., & Deifalla, A. (2021). Prediction of shear strength of FRP reinforced beams with and without stirrups using (GP) technique. Ain Shams Engineering Journal, 12(3), 2493–2510. doi:10.1016/j.asej.2021.02.006.

[23] Ebid, A. M., Deifalla, A. F., & Mahdi, H. A. (2022). Evaluating Shear Strength of Light-Weight and Normal-Weight Concretes through Artificial Intelligence. Sustainability (Switzerland), 14(21), 14010. doi:10.3390/su142114010.